ELSEVIER

Journal of Power Sources 62 (1996) 9–14

JOURNAL OF POWER SOURCES

Performance characterization of sintered iron electrodes in nickel/iron alkaline batteries

P. Periasamy, B. Ramesh Babu, S. Venkatakrishna Iyer

Central Electrochemical Research Institute, Karaikudi 630 006, India

Received 1 December 1995; accepted 29 January 1996

Abstract

A nickel/iron storage battery with a porous, sintered, iron negative electrode and a nickel positive electrode is a high power system by virtue of its low internal resistance. A dry-powder sintering procedure is used to fabricate negative and positive electrodes. Negative iron electrodes are activated with various salt solutions such as $CdSO_4$, $BaCl_2$, $HgCl_2$ and sulfur. Positive electrodes are impregnated with nickel hydroxide by a chemical method. Tests are performed in 10 Ah capacity nickel/iron cells and two types of activated iron electrodes are used. The present work deals with electrode fabrication, charge/discharge studies, self-discharge, temperature performance and cycle life. Finally, the best iron electrodes are coupled with nickel electrodes to obtain a 1.37 V, 75 Ah nickel/iron cell. The performance of this cell is discussed.

Keywords: Electrodes; Iron; Nickel; Alkaline batteries

1. Introduction

The nickel/iron battery is a rechargeable electrochemical power source. Such a battery with sintered electrodes offers fairly high specific energy and specific power — parameters that are essential for electric-vehicle propulsion. The iron electrode has a low hydrogen overvoltage; the ionization potential and hydrogen evolution potential are very close to each other in an alkaline medium. Iron electrodes have been prepared by introducing additives into iron powder or by incorporating additives by electro-chemical methods [1]. The performance can be improved by mixing additives with iron oxide powder [2]. An advanced nickel/iron battery with an energy density of 55–80 Wh kg^{-1} has been used as a power source for an electric vehicle [3,4]. The self-discharge of the nickel/iron battery is 2–3% of the nominal capacity at 300 K [5]. The present work deals with the electrode fabrication, the activation of both positive and negative electrodes, and the assembly and testing of cells.

2. Experimental

2.1. Preparation of sintered iron negative electrodes

Electrolytic iron powder of −300 mesh was spread uniformly over a nickel-plated, iron-wire mesh substrate (0.12 mm thickness) kept in a graphite die. The electrode was sintered in the 1173–1223 K temperature range for 30 min under a hydrogen atmosphere. Iron and iron–copper electrodes (12 cm × 10 cm × 0.15 cm) were impregnated cathodically with a 0.1 M solution of mercuric chloride as described in Ref. [6]. Sulfur was impregnated (from 5.35 M KOH + 0.5 M sulfur solution) on the sintered iron and iron–copper activated electrodes. The impregnation was effected by applying a cathodic current of 20 mA for 15 min. The quantity of deposited metal was obtained from the increase in the weight of the electrodes. The composition of the iron-activated electrodes obtained in this way are given in Table 1.

Table 1
Composition (wt.%) of iron electrodes

Electrode	Composition
B	100% porous iron
G	98% Fe + 2% S
CG	90% Fe + 8% Cu + 2% S
CGD	82% Fe + 8% Cu + 8% Cd + 2% S
CGE	81% Fe + 8% Cu + 9% BaO + 2% S
CGF	81% Fe + 8% Cu + 9% Hg + 2% S

2.2. Preparation of sintered nickel positive electrodes

Porous nickel electrodes were prepared from carbonyl nickel powder. The nickel matrix was prepared using a grid

PII S0378-7753(96)02391-9

of the same size as that of the iron electrode, and sintered under a hydrogen atmosphere at 1148–1198 K for 30 min. Electrodes of porosity 80–85% were subjected to cathodic treatment for incorporating nickel hydroxide. Impregnation was carried out by immersing the electrode in 4 M $Ni(NO_3)_2$ + 5% $Co(NO_3)_2$ solution. The electrode was then transferred to a hot alkaline solution and cathodically treated as described in Ref. [7]. The process was repeated until a sufficient loading of $Ni(OH)_2$ was achieved. The electrode obtained in this way was made free of nitrate ions by washing it several times with water, and then it was thoroughly dried.

2.3. Formation process

Sintered iron and activated iron electrodes and two excess capacity nickel electrodes, with nylon cloth as the separator, were used for the formation process. The electrolyte solution was 5.35 M KOH + 0.65 M LiOH (base electrolyte (BE)) + 0.01 M Na_2S. The iron working electrodes were charged at the $C/4$ rate and discharged at the $C/8$ rate to a cutoff voltage −0.8 V versus Hg/HgO, OH^- reference electrode.

2.4. Charge/discharge characteristics of 10 Ah cells

Two types of sintered iron electrodes have been used (G and CGF) to conduct studies for obtaining various electrochemical parameters.

2.4.1. Charging at different rates and discharging at a constant rate

The variation of iron electrode potential versus capacity was measured using electrodes G (98% Fe + 2% S) and CGF (81% Fe + 8% Cu + 9% Hg + 2% S). These electrodes were charged at different rates, such as $C/5$, $C/2.5$, $C/1.66$ and $C/1.33$, and discharged at the $C/2$ rate in BE + 0.01 M Na_2S solution.

2.4.2. Charging at a constant rate and discharging at different rates

The variation of iron electrode potential versus capacity was measured for electrodes G and CGF. They were charged at the $C/2$ rate and discharged at different rates, such as $C/5$, $C/1.66$ and $C/1.33$, in BE + 0.01 M Na_2S solution.

2.4.3. Self-discharge studies of iron electrodes

The variation of electrode potential versus capacity was measured for electrodes G and CGF after 24, 72, 120 and 240 h in BE + 0.01 M Na_2S solution.

2.4.4. Study of discharge characteristics at different temperatures

The variation of electrode potential versus capacity was measured for electrodes G and CGF at temperatures of 333, 303, 263, 248 and 233 K in BE + 0.01 M Na_2S.

2.4.5. Study of the performance of a 1.37 V, 75 Ah Ni–Fe cell

The 75 Ah cell employed six activated iron negative electrodes (CGF) and five nickel hydroxide positive electrodes. The electrodes were arranged alternately with nylon cloth as the separator in between. A common terminal was provided for all the positive and negative electrodes. The electrode stack was immersed in BE + 0.01 M Na_2S solution. The assembled cell was charged at the $C/2$ rate and discharged at the C, $C/2$ and $C/4$ rates.

3. Results and discussion

The variation of the capacity of the sintered iron electrode and activated electrodes with increase in the number of cycles in BE + 0.01 M Na_2S solution is shown in Fig. 1. On the basis of capacity, the performance of different electrodes at the end of the tenth cycle is: CGF > G > CGE > B > CGD > CG. The formation process has been considered [8,9] to be an important pre-requisite in the fabrication of iron electrodes for alkaline batteries. Therefore, it is concluded that seven to ten cycles are sufficient for the formation of sintered iron electrodes.

The variation of electrode potential versus capacity for electrodes G and CGF at different rates are given in Figs. 2

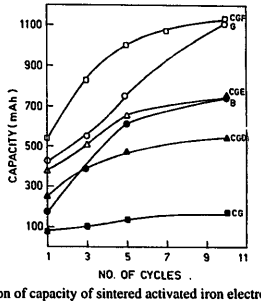

Fig. 1. Variation of capacity of sintered activated iron electrodes in 5.35 M KOH + 0.65 M LiOH + 0.01 M Na_2S solution.

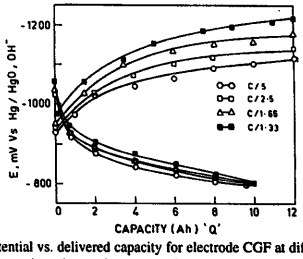

Fig. 2. Potential vs. delivered capacity for electrode CGF at different rates of charging ($C/5$, $C/2.5$, $C/1.66$ and $C/1.33$) and discharged at $C/2$ rate in 5.35 M KOH + 0.65 M LiOH + 0.01 M Na_2S solution.

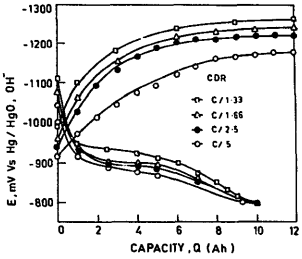

Fig. 3. Potential vs. delivered capacity for the electrode G at different rates of charging (*C*/5, *C*/2.5, *C*/1.66 and *C*/1.33) and discharged at *C*/2 rate in 5.35 M KOH + 0.65 M LiOH + 0.01 M Na_2S solution.

and 3, respectively. The data show that different rates of charging lead to the attainment of different maximum potentials. The maximum potential increases with increase in the charging current. The electrode potential falls by about 250 mV during the first delivery of 80% capacity at the *C*/1.33 rate for CGF electrode. The same electrode is found to deliver lower capacity, i.e. 60 to 70% at the *C*/1.66, *C*/2.5 and *C*/5 rates. A similar behaviour is observed for the G electrode. The electrode potential falls by about 250 mV during the first delivery of 60% capacity at the *C*/1.33 rate. The same electrode is found to show lower capacity at the *C*/1.6, *C*/2.5 and *C*/5 rates. In view of this performance of the CGF and G electrodes, it is found that the rate of charging increases from *C*/5 to *C*/1.33 rates and that the output automatically increases with constant rate of discharge at the *C*/5 rate. Finally, the output of the CGF electrode is higher than that of the G electrode at the first discharge step of conversion of $Fe \rightarrow Fe(OH)_2$ at the *C*/1.33 rate.

The change in electrode potential with capacity for electrodes G and CGF at a constant rate of charging and with different rates of discharging (namely, *C*/5, *C*/1.66 and *C*/1.33) is presented in Fig. 4. The potential of the CGF electrode falls by about 150 mV during delivery of 93, 65

Table 2
Parameters derived from discharge at a constant rate and charge at different rates

Electrode	Charge rate	$(dE/dQ)_{Q=50\%} \times 10^{-3}$ VC^{-1}
G	*C*/5	15
G	*C*/2.5	10
G	*C*/1.66	10
G	*C*/1.33	7
CGF	*C*/5	10
CGF	*C*/2.5	8
CGF	*C*/1.66	5
CGF	*C*/1.33	5

Table 3
Parameters derived from discharge at different rates

Electrode	Discharge rate	$(dE/dQ)_{Q=50\%} \times 10^{-3}$ VC^{-1}
G	*C*/5	25
G	*C*/1.66	12.5
G	*C*/1.33	10.5
CGF	*C*/5	9
CGF	*C*/1.66	10
CGF	*C*/1.33	15

and 55% of the capacity at the *C*/5, *C*/1.66 and *C*/1.33 rates, respectively. Similar behaviour is exhibited by the electrode G during the delivery of 72, 33 and 23% of the capacity at the *C*/5, *C*/1.66 and *C*/1.33 rates, respectively.

The parameters derived from the discharge curves at different and constant rates in BE + 0.01 M Na_2S solution are listed in Tables 2 and 3. An ideal reversible battery requires the slope of the open-circuit potential versus the state-of-discharge curve (E versus Q) to be zero, in the absence of overpotential, diffusion potential and internal resistance. Therefore, $(dE/dQ$ at 50% state-of-discharge, i.e. $(dE/dQ)_{Q=50\%}$, was used to compare the reversible behaviour of the electrode [10]. It is seen from the Table 2 that $(dE/dQ)_{Q=50\%}$ values of more than zero are obtained for electrodes G and CGF when they are charged at different rates

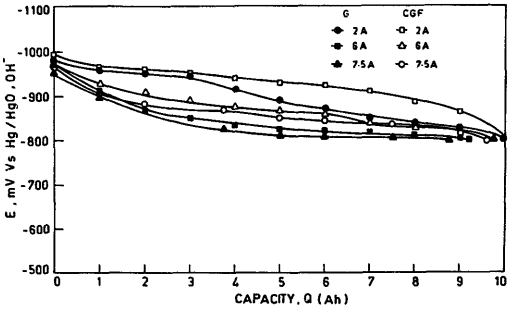

Fig. 4. Potential vs. delivered capacity for electrodes G and CGF at constant rate of charging with different rates of discharging (*C*/5, *C*/1.66 and *C*/1.33) in 5.35 M KOH + 0.65 M LiOH + 0.01 M Na_2S solution.

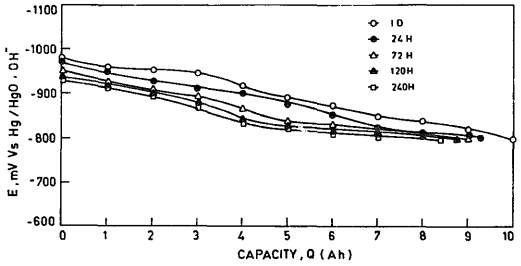

Fig. 5. Potential vs. capacity for electrode G and after 24, 72, 120 and 240 h in 5.35 M KOH + 0.65 M LiOH + 0.01 M Na_2S solution.

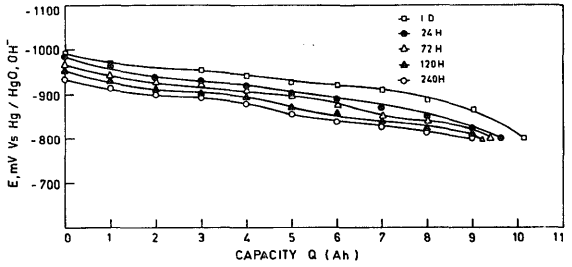

Fig. 6. Potential vs. capacity for the electrode CGF after 24, 72, 120 and 240 h in 5.35 M KOH + 0.65 M LiOH + 0.01 M Na_2S solution.

Table 4
Self-discharge characteristics of 10 Ah iron electrodes

Electrode	Time (h)	Loss in nominal capacity (%)
G	24	6.8
G	72	10.0
G	120	12.8
G	240	18
CGF	24	3.4
CGF	72	4.4
CGF	120	5.8
CGF	240	10.0

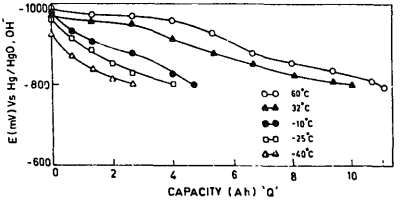

Fig. 7. Potential vs. capacity for electrode G at temperature −40, −25, 0, 32 and 60 °C in 5.35 M KOH + 0.65 M LiOH + 0.01 M Na_2S solution.

and discharged at a constant rate. The $(dE/dQ)_{Q=50\%}$ values are found to decrease with increase in the rate of charging. This may be due to the incorporation of sulfur on the surface at higher rates of charging. It has already been reported [11] that the incorporation of sulfur hinders the hydrogen evolution reaction by increasing the Fe–H bond energy. From the data given in Table 3, it can be seen that the value of $(dE/dQ)_{Q=50\%}$ decreases with increase in the rate of discharging. Moreover, the lower the value $(dE/dQ)_{Q=50\%}$, the better will be the reversibility of the electrode. Thus, electrode charging at higher rates will be more reversible.

The variation of potential versus capacity for electrodes G and CGF after 24, 72, 120 and 240 h in BE + 0.01 M Na_2S solution is given in Figs. 5 and 6, respectively. The self-discharge increases with the residence time. Self-discharge is minimum for 24 h and maximum for 240 h for both electrodes. The nominal loss of capacity increases with increase in time for both electrodes, see Table 4. The loss is less for the electrode CGF.

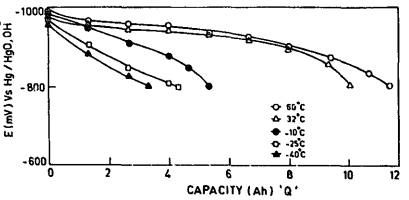

Fig. 8. Potential vs. capacity for electrode CGF at temperature −40, −25, 0, 32, and 60 °C in 5.35 M KOH + 0.65 M LiOH + 0.01 M Na_2S solution.

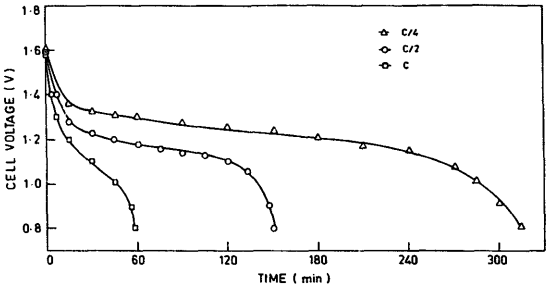

Fig. 9. Cell potential vs. time discharge at different rates (*C*, *C*/2 and *C*/4) for a 75 Ah nickel–iron cell.

The influence of temperature on the discharge characteristics of electrodes G and CGF is shown in Figs. 7 and 8, respectively. There is an decrease in both the electrode potential and the capacity as the temperature is decreased from 333 to 233 K. Several studies [12,13] have shown that charge and discharge reactions for a porous iron electrode in an alkaline solution proceed via the following intermediates

$$Fe \rightarrow HFeO_2^- \rightarrow Fe(OH)_2 \quad (1)$$

$$Fe(OH)_2 \rightarrow HFeO_2^- \rightarrow FeO_2^- \rightarrow FeOOH \quad (2)$$

At temperatures above 323 K, a direct oxidation of $Fe \rightarrow FeOOH$ in the dissolved species occurs

$$Fe + 2H_2O \rightarrow FeOOH + 3H^+ + 2e^- \quad (3)$$

At a temperature of 273 K and below, the two reactions (namely, the reduction of $Fe(OH)_2$ and hydrogen evolution) seem to overlap. The higher the conductivity of the solid phase, the larger will be the electrode capacity. The increase in capacity with increase in temperature is probably due to improved ionic conductivity of ferrous hydroxide film on the electrode [14].

Table 5 gives the influence of temperature on the parameters derived from cell performance curves for electrodes G and CGF in BE + 0.1 M Na_2S. The $(dE/dt)_{Q=50\%}$ value is minimum for the G and CGF electrodes at 333 K and maximum at 303 and 263 K.

Table 5
Parameters derived from discharge at *C*/5 rate

Electrode	Temperature	$(dE/dQ)_{Q=50\%} \times 10^{-3}$ VC^{-1}
G	333	15
G	303	30
G	263	
G	248	
G	233	
CGF	333	10
CGF	303	10
CGF	263	35
CGF	248	
CGF	233	

The discharge curves, i.e. voltage versus time plots, at different rates in BE + 0.01 M Na_2S solution are presented in Fig. 9.

The general performance of the prototype nickel/iron cell is as follows

Open-circuit potential	1.37 V
Operating voltage	1.3 to 0.8 V
Size of negative electrode dimensions	16 cm × 14 cm × 0.12 cm
Size of positive electrode dimensions	16 cm × 14 cm × 0.15 cm
Cell assembly weight with electrolyte	2.6 kg
Energy density	33 Wh kg^{-1} at *C*/4 rate
Charge/discharge efficiency	75%
Cycle life	750 cycles at *C*/4 rate

The energy efficiency and cycle life achieved for the sintered nickel–iron cells are fairly good.

4. Conclusions

The formation process is found to improve the performance of iron electrodes. Electrodes such as 98% Fe + 2% S (G) and 81% Fe + 8% Cu + 9% Hg + 2% S (CGF) have been found to show good performance, in terms of capacity, at the end of tenth cycle. The electrodes give (dE/dQ) values that are greater than zero and, accordingly, they approach the ideal reversible behaviour required for a battery electrode.

An increase in capacity with increase in temperature is observed. This may be due to improved ionic conductivity of the ferrous hydroxide film on the electrode.

Electrodes G and CGF in contact with 5.35 M KOH + 0.65 M LiOH + 0.01 M Na_2S serve as the best battery electrodes in alkaline media.

Acknowledgements

Authors are thankful to the Director, CECRI, for his keen interest in this work and also for his kind permission to publish this paper.

References

[1] C. Chakkaravarthy, P. Periasamy, S. Jegannathan and K.I. Vasu, *J. Power Sources, 35* (1991) 21.
[2] K. Micka and Z. Zabransky, *J. Power Sources, 19* (1987) 315.
[3] T. Iwaki, T. Mitsumata and H. Ogawa, *Prog. Batteries Fuel Cells, 4* (1982) 255.
[4] J. Labat, *Prog. Batteries Fuel Cells, 6* (1987) 236.
[5] J. McBreen, *NTIS Rep. De 84 010 963 on Secondary Alkaline Batteries*, 1984.
[6] B. Ramesh Babu, P. Periasamy and C. Chakkaravarthy, *Bull. Electrochem., 9* (1993) 371.
[7] M. Jayalakshmi, B. Nithira Begum, V.R. Chidambaram, R. Sabapathi and V.S. Muralidharan, *J. Power Sources, 39* (1992) 113–119.
[8] K. Vijayamohanan, A.K. Shukla and S. Sathyanarayana, *Indian J. Technol., 24* (1986) 436.
[9] K. Vijayamohanan, A.K. Shukla and S. Sathyanarayana, *J. Power Sources, 32* (1990) 329.
[10] V.S. Muralidharan, M. Ramakrishnan, G. Paruthimal Kalaignan, K. Gopalakrishnan and K.I. Vasu, *J. Power Sources, 27* (1989) 311.
[11] G. Paruthimal Kalaignan, V.S. Muralidharan and K.I. Vasu, *Proc. 10th Int. Congr. Metallic Corrosion, Madras, India, 7–11 Nov. 1987*. Vol. 1, Oxford and IBH Publishing, New Dehli, 1987, p. 615.
[12] R.D. Armstrong and I. Baurhoo, *J. Electroanal. Chem., 34* (1972) 41.
[13] L. Ojefors, *J. Electrochem. Soc., 123* (1976) 1139.
[14] P.R. Vassie and A.C.C. Tseung, *Electrochim. Acta, 21* (1976) 299.